Reflection coefficients and screech-tone prediction in supersonic jets

Matteo Mancinelli, Vincent Jaunet, Peter Jordan, Aaron Towne, Steve Girard

▶ **To cite this version:**

Matteo Mancinelli, Vincent Jaunet, Peter Jordan, Aaron Towne, Steve Girard. Reflection coefficients and screech-tone prediction in supersonic jets. 25th AIAA/CEAS Aeroacoustics Conference, May 2019, Delft, Netherlands. 10.2514/6.2019-2522 . hal-02378551

HAL Id: hal-02378551
https://hal.science/hal-02378551

Submitted on 25 Nov 2019

HAL is a multi-disciplinary open access archive for the deposit and dissemination of scientific research documents, whether they are published or not. The documents may come from teaching and research institutions in France or abroad, or from public or private research centers.

L'archive ouverte pluridisciplinaire **HAL**, est destinée au dépôt et à la diffusion de documents scientifiques de niveau recherche, publiés ou non, émanant des établissements d'enseignement et de recherche français ou étrangers, des laboratoires publics ou privés.

Reflection coefficients and screech-tone prediction in supersonic jets

Matteo Mancinelli*
Institut Pprime, CNRS-Université de Poitiers-ENSMA, 86962 Chasseneuil du Poitou, Poitiers, France
Direction des Lanceurs, CNES, 75612 Paris, France

Vincent Jaunet† and Peter Jordan‡
Institut Pprime, CNRS-Université de Poitiers-ENSMA, 86962 Chasseneuil du Poitou, Poitiers, France

Aaron Towne§
University of Michigan, Ann Arbor, MI 48109, USA

Stève Girard¶
Institut Pprime, CNRS-Université de Poitiers-ENSMA, 86962 Chasseneuil du Poitou, Poitiers, France

We study and model the resonance mechanism underlying the generation of A1 and A2 screech modes in an under-expanded supersonic jet. Following our previous work [1], where upstream-travelling guided jet modes were used to provide closure of the screech resonance loop, we here consider a more complete model in which both wavenumbers and frequencies of the upstream- and downstream-travelling waves are complex. The new model requires knowledge of the upstream and downstream reflection coefficients, which are treated as parameters and identified using the experimental data. The new screech model is shown to provide a more complete description of the measured data.

I. Nomenclature

c_∞	=	Ambient speed of sound
k	=	Dimensionless streamwise wavenumber
ω	=	Non-dimensional frequency
m	=	Order of the azimuthal Fourier mode
n_r	=	Radial order of the guided jet modes
St	=	Nozzle diameter-based Strouhal number
M_a	=	Acoustic Mach number
M_j	=	Jet Mach number
U_j	=	Jet velocity
T	=	Jet-to-ambient temperature ratio
k_{KH}	=	Kelvin-Helmholtz instability mode
k_p	=	Guided jet mode
L_1	=	Length of the first shock cell
L_s	=	Location of the s^{th} shock cell
Re	=	Nozzle diameter-based Reynolds number
D	=	Nozzle diameter
r	=	Radial distance from the nozzle axis
$SPSL$	=	Sound Pressure Spectrum Level
R_1R_2	=	Reflection coefficient product

*Post-doctoral Research Fellow, Département Fluides Thermique et Combustion, 11 Boulevard Marie et Pierre Curie.
†Assistant Professor, Département Fluides Thermique et Combustion, 11 Boulevard Marie et Pierre Curie.
‡Researcher, Département Fluides Thermique et Combustion, 11 Boulevard Marie et Pierre Curie.
§Assistant Professor, Department of Mechanical Engineering, 2350 Hayward Street.
¶Research Engineer, Département Fluides Thermique et Combustion, 11 Boulevard Marie et Pierre Curie.

II. Introduction

The generation and modelling of screech noise in non-perfectly expanded supersonic jets is a long-standing issue. According to Powell *et al.* [2], the screech-frequency evolution with the jet Mach number is characterised by the jump into different modes or stages, namely axisymmetric A1 and A2 modes, flapping B and D modes and helical C mode.

It is known that screech is a resonance phenomenon due to a feedback mechanism loop involving a downstream-travelling flow disturbance generated at the nozzle exit and an upstream-travelling wave generated by the interaction of the flow disturbance with the shock-cell pattern. Since the seminal work of Powell [3], it has been assumed that the closure mechanism of the screech loop is provided by a free-stream acoustic wave. On the basis of this phenomenological description of the screech mechanism, several screech-frequency prediction models have been proposed [3–6]. The idea that screech may not be closed by free-stream acoustic waves was first suggested by Shen & Tam [7], who claimed that A1 and B screech modes involved free-stream acoustic waves, whereas A2 and C modes involved upstream-travelling guided jet modes. These modes were first studied by Tam & Hu [8] and have been exploited to explain many resonance phenomena in jets (resonances occurring in subsonic and supersonic impinging jets [9, 10], weak resonances in high-speed subsonic jets [11], high-amplitude tone appearance in jet-flap interaction configuration [12]). Most importantly, they have been shown to be active in screeching supersonic jets [13, 14]. Given this observation, we recently developed a screech-frequency prediction model based on a resonance between downstream-travelling Kelvin-Helmholtz (K-H) wave and upstream-travelling guided jet modes [1]. Both K-H and upstream-travelling jet waves were computed via a cylindrical vortex-sheet model. Contrary to the assertions of Shen & Tam [7], we showed that both A1 and A2 screech modes are underpinned by a resonance involving the said upstream-travelling modes. The predictions obtained provide better agreement with experimental data than does the classical screech-prediction approach using free-stream acoustic waves.

In the said model, and consistent with what is frequently assumed when considering fluid-mechanics resonance phenomena [12], we assumed that the upstream- and downstream-travelling waves are both spatially neutrally stable. With these assumptions, knowledge of the magnitude of the reflection coefficients is not necessary for screech-frequency predictions. While predictions provide good agreement with data, the simplification misses certain aspects of the real behaviour of screech.

We thus here consider an improved screech-tone prediction model which brings us to focus on the upstream and downstream reflection mechanisms involved in screech. The model is based on a complex frequency-wavenumber analysis. The assumption of spatially neutrally stable waves is thus dropped. Both the magnitude and phase of the reflection coefficient product come into play in determination of the resonance frequency. The reflection coefficient product is an unknown function of both frequency and flow conditions. We therefore treat it as a parameter and we explore the prediction results obtained by imposing its amplitude and phase. On the basis of the results obtained, we propose a functional form of the reflection coefficient product as a function of both frequency and jet Mach number.

The paper is organised as follows. The resonance model is presented in §III. §IV describes the experimental setup and the instrumentation adopted. Main results concerning the screech-frequency predictions and the estimation of the reflection coefficient product are reported in §V. Conclusions and future developments of the research activity are discussed in §VI.

III. Resonance model

In this section we present the model based on a resonance between downstream-travelling K-H instability wave and upstream-travelling guided jet modes. Following Towne *et al.*[11] and Mancinelli *et al.*[1], we use the terms downstream- and upstream-travelling to designate the sign of the group velocity. Accordingly, the downstream- and upstream-travelling waves are indicated with superscripts + and −, respectively. The notation used in the manuscript is reported in the following for the sake of clarity. The Kelvin-Helmholtz instability is denoted k_{KH} and the guided jet modes k_p.

A. Cylindrical vortex-sheet model

The linear dynamics of the waves is modelled via a cylindrical vortex sheet [15, 16]. Following our previous work [1], the normal mode ansatz is:

$$q(x, r, \theta, t) = \hat{q}(r)\, e^{i(kx+m\theta-\omega t)}, \tag{1}$$

where k is the streamwise wavenumber normalised by the nozzle diameter D, m the azimuthal mode and ω the dimensionless frequency $\omega = 2\pi St M_a$, with $St = fD/U_j$ the nozzle-diameter-based Strouhal number and $M_a = U_j/c_\infty$ the acoustic Mach number. The vortex-sheet dispersion relation is:

$$D\left(k,\omega;M_a,T,m\right) = \frac{1}{\left(1-\frac{kM_a}{\omega}\right)^2} + \frac{1}{T}\frac{I_m\left(\frac{\gamma_i}{2}\right)\left(\frac{\gamma_o}{2}K_{m-1}\left(\frac{\gamma_o}{2}\right)+mK_m\left(\frac{\gamma_o}{2}\right)\right)}{K_m\left(\frac{\gamma_o}{2}\right)\left(\frac{\gamma_i}{2}I_{m-1}\left(\frac{\gamma_i}{2}\right)-mI_m\left(\frac{\gamma_i}{2}\right)\right)} = 0, \tag{2}$$

with

$$\gamma_i = \sqrt{k^2 - \frac{1}{T}\left(\omega - M_a k\right)^2}, \tag{3a}$$

$$\gamma_o = \sqrt{k^2 - \omega^2}, \tag{3b}$$

where I and K are modified Bessel functions of the first and second kind, respectively, and T is the jet-to-ambient temperature ratio T_j/T_∞, so that the relation between the acoustic and jet Mach numbers is given by $M_j = U_j/c_j = M_a/\sqrt{T}$. The branch cut of the square root in eqs. (3a) and (3b) is chosen such that $-\pi/2 \leq \arg\left(\gamma_{\mathrm{i,o}}\right) \leq \pi/2$.

According to Towne *et al.* [11], k_p modes belong to a hierarchical family of waves identified by their azimuthal and radial orders m and n_r, respectively. We restrict attention to azimuthal mode $m = 0$ due to the axisymmetry property of screech modes A1 and A2, and we let vary the radial order in the range $n_r = 1, 2$. We assume isothermal conditions in the modelling, i.e. $T = 1$. Frequency/wavenumber pairs (ω, k) that satisfy eq. (2) define eigenmodes of the vortex sheet for given values of m, M_a and T. To find these pairs, we specify a frequency ω and compute the associated eigenvalues k according to eq. (2).

In our previous work [1], $\omega \in \mathcal{R}$, consequently $k^+_{KH} \in C$ and $k^-_p \in \mathcal{R}$. Then a neutral mode assumption was made in order to compute resonance-frequency predictions neglecting the imaginary part of the K-H instability wave. In this paper we consider a complex frequency $\omega \in C$, this implies that both downstream- and upstream-travelling waves $k^+_{KH}, k^-_p \in C$. In the complex-frequency analysis, eigenvalues must satisfy the dispersion relation (2) and at the same time the constraint imposed by the magnitude of the reflection coefficient product that is described in the next section.

B. Resonance conditions

In this section we discuss the conditions that k^+_{KH} and k^-_p must satisfy in order for resonance to occur. We assume that waves exchange energy upstream at the nozzle exit and downstream at the s^{th} shock-cell location where an interaction between the K-H instability wave and the shock-cell pattern occurs. According to the results we obtained in our previous work [1] and in agreement with results reported in the literature [17], we consider the fourth shock-cell as downstream reflection point, i.e. $s = 4$. The location of the s^{th} shock cell is given by the Pack's model [18]:

$$L_1\left(M_j\right) = \frac{\pi}{2.4048}\sqrt{M_j^2 - 1}, \tag{4a}$$

$$L_s\left(M_j\right) = L_1\left(\left(1-\alpha\right)s + \alpha\right), \tag{4b}$$

where L_1 is the length of the first shock cell, L_s the s^{th} shock-cell location and α the rate of decrease of the shock-cell length with the downstream distance, whose value was set to 0.06 according to Harper-Bourne [19]. Following Landau & Lifshitz [20], the condition to be satisfied for resonance to occur is:

$$R_1 R_2 e^{i\Delta k L_s} = 1, \tag{5}$$

where $R_1\left(St, M_j\right) \in C$ and $R_2\left(St, M_j, L_s\right) \in C$ are the reflection coefficients at the nozzle exit and shock-cell location, respectively. Following Jordan *et al.* [12], eq. (5) can be rewritten in terms of magnitude and phase constraints,

$$e^{\Delta k_i L_s} = |R_1 R_2|, \tag{6a}$$

$$\Delta k_r L_s + \phi = 2p\pi, \tag{6b}$$

where ϕ is the phase of the reflection coefficient product.

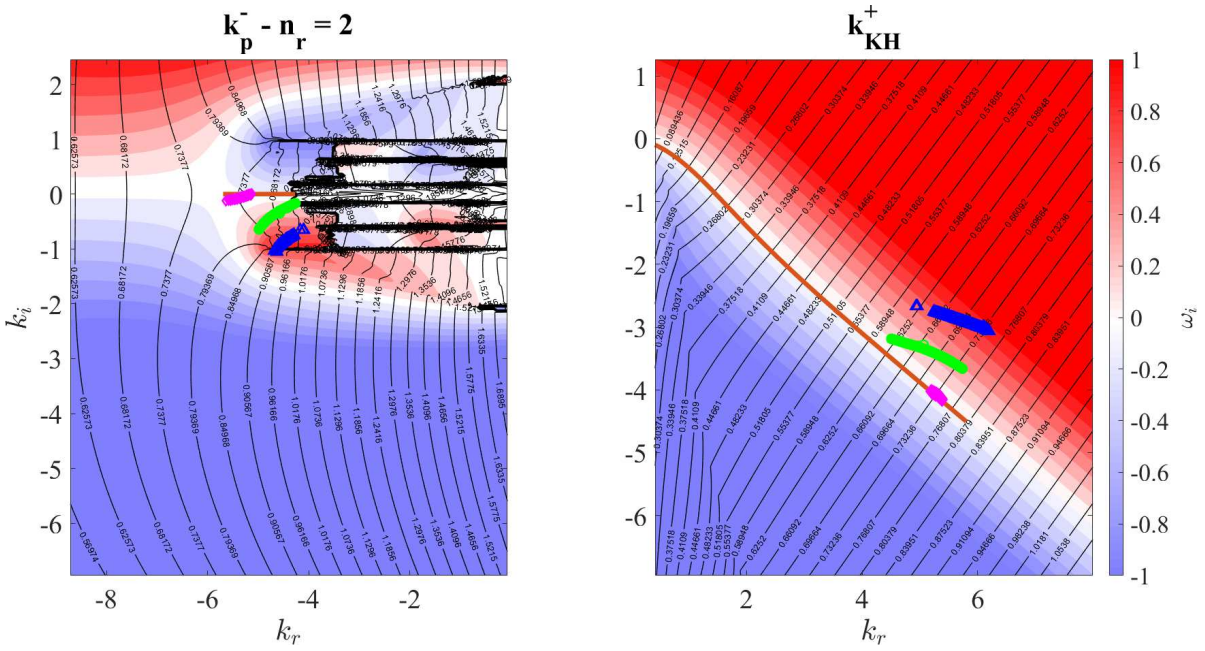

Fig. 1 Vortex-sheet solutions for both k_{KH}^+ and k_p^- satisfying eq. (2) for azimuthal mode $m = 0$ and fully expanded jet Mach number $M_j = 1.1$. Upstream-travelling modes for $n_r = 2$ are here considered. The colour map shows ω_i, whereas the black contour represents $St = \omega_r/2\pi M_a$. Solid brown lines represent the eigenvalues in the case of real frequency analysis. Markers represent eigenvalues satisfying both the dispersion relation (2) and the magnitude constraint (6a) for $s = 4$ and different values of $|R_1R_2|$: magenta $\diamond$ refer to $|R_1R_2| = 10^{-4}$, green $\circ$ to $|R_1R_2| = 10^{-3}$, blue $\triangle$ to $|R_1R_2| = 10^{-2}$.

Perform resonance-frequency predictions involves finding triplets $\left[k_{KH}^+, k_p^-, \omega\right] \in C$ simultaneously satisfying eqs. (2), (6a) and (6b). This implies the knowledge of the reflection coefficient product as a function of both frequency and jet Mach number. Given that we do not have any knowledge about R_1R_2, we use the reflection coefficient product as a parameter of the model, we assign a value to it and we solve eqs. (2) and (6a) to find complex frequencies and eigenvalues constrained by the magnitude of the reflection coefficient product. Then we use the phase constraint in eq. (6b) to select resonance frequency. Following our previous work [1], we explore the extreme conditions $\phi = 0$ and $\phi = -\pi$. According to the results we found in Mancinelli *et al.* [1], we observed the best agreement with the experimental data by considering out-of-phase reflection conditions, which leads to the following resonance criterion,

$$Re\left[k_{KH}^+ - k_p^-\right] = \Delta k_r = \frac{(2p+1)\,\pi}{L_s}. \tag{7}$$

Figure 1 shows the vortex-sheet solutions $\omega(k)$ for both downstream- and upstream-travelling waves for azimuthal mode $m = 0$, fully expanded jet Mach number $M_j = 1.1$ and fourth shock-cell location as downstream reflection point. Eigenvalues obtained from both real- and complex-frequency analyses are represented, with k_{KH}^+ and k_p^- satisfying both eqs. (2) and (6a) for $\omega \in C$. We consider upstream-travelling modes of second radial order, i.e. $n_r = 2$. Eigenvalues are computed for three constant values of reflection coefficient product amplitude: $|R_1R_2| = 10^{-4}$, 10^{-3} and 10^{-2}. We point out that both downstream- and upstream-travelling waves are characterised by $k_i < 0$ for $\omega \in C$, thus implying that k_{KH}^+ and k_p^- are spatially unstable and evanescent, respectively. We observe that for $\omega \in C$ the eigenvalues bend in the k_i-k_r plane towards regions of positive imaginary frequency with respect to the eigenvalues obtained for $\omega \in \mathcal{R}$. Indeed, values of $\omega_i \lesseqgtr 0$ represents attenuation/amplification in time of the resonance feedback loop. Eigenvalues satisfying both eqs. (2) and (6a) are therefore eigenvalues that, for the given value of $|R_1R_2|$, are characterised by positive values of ω_i to sustain resonance.

Figure 2 represents the resonance-frequency selection by imposing out-of-phase reflection conditions (7) for $m = 0$ and $M_j = 1.1$. We consider the amplitude of the reflection coefficient product equal to 10^{-1} and 10^{-3} for k_p^- modes of the first and second radial orders, respectively.

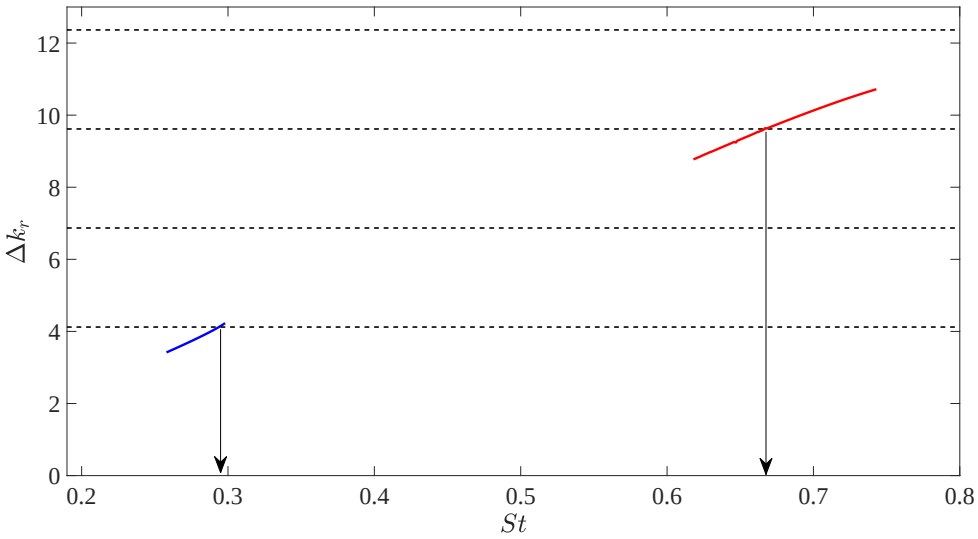

Fig. 2 Resonance-frequency selection for $m = 0$, $M_j = 1.1$. Blue line refers to Δk_r for k_p^- with $n_r = 1$ and $|R_1 R_2| = 10^{-1}$, red line to Δk_r for k_p^- with $n_r = 2$ and $|R_1 R_2| = 10^{-3}$. Horizontal dashed black lines refer to resonance criteria in the case of out-of-phase reflection conditions (7)**.**

IV. Experimental set-up

The experimental test campaign was performed at the *SUCRÉ* (SUpersoniC REsonance) jet noise facility in the *Prométée* technological platform of the *Institut Pprime* in Poitiers. The supersonic under-expanded jet issues from a simple convergent nozzle of diameter $D = 0.01m$. Experimental tests were carried out for a stagnation pressure range $p_0 = [1.89, 5.75]$ with a corresponding fully expanded jet Mach number range $M_j = [1, 1.8]$ and a nozzle diameter-based Reynolds number range $Re = U_j D/\nu = \left[2.86 \cdot 10^5, 7.9 \cdot 10^5\right]$. The tests were performed with a very fine resolution $\Delta M_j = 0.005$ for $M_j = [1, 1.3]$ in order to capture the fine details of the Mach-number dependence of screech modes A1 and A2, and with a resolution $\Delta M_j = 0.01$ for $M_j = [1.31, 1.8]$.

Pressure fluctuations were measured by GRAS 46BP microphones, whose frequency response is flat in the range $4\,Hz$-$70\,kHz$. Data were acquired by a National Instruments PXIe-1071 acquisition card with a sampling frequency of $200\,kHz$ which provides a maximum resolved Strouhal number range $[2, 3.2]$ well above the St of interest in this paper. The acquisition time was set equal to $30\,s$, which is six orders of magnitude larger than the longest convective time, thus ensuring statistical convergence of the quantities presented in the paper [21]. An azimuthal array of six microphones was placed in the nozzle exit plane and radial distance $r/D = 1$. Such a device allowed to resolve the most energetic azimuthal Fourier modes: $m = 0, \pm 1, \pm 2$. A schematic representation of the experimental setup and microphone disposition is depicted in figure 3. For more details on the jet facility and experimental setup the reader can refer to Mancinelli *et al.*[1].

V. Results

Figure 4 shows the Sound Pressure Spectrum Level [1, 22, 23] in dB/St as a function of St and M_j for azimuthal mode $m = 0$. Signature of screech modes A1 and A2 are detected at high frequencies in the jet Mach number range $[1.07, 1.24]$. A weaker low-frequency peak is detected as well for almost all the jet Mach numbers and its intensity rises with increasing M_j. Furthermore, we unexpectedly detect the footprint of the asymmetric B, C and D modes in the middle-frequency range. Indeed, the rising up of these asymmetric modes in the azimuthal mode $m = 0$ results from the non-linear interaction between azimuthal modes $m = +1$ and $m = -1$, as shown in the appendix. Hence, we did not take into account the signature of the B, C and D modes in the screech modelling of $m = 0$ mode and we focused on the predictions of screech modes A1 and A2 and on the low-frequency energy peak.

Figure 5 shows the spectral maps of $m = 0$ mode and the screech-frequency predictions obtained using the resonance model presented in §III. Predictions are obtained considering the fourth shock cell as downstream reflection point,

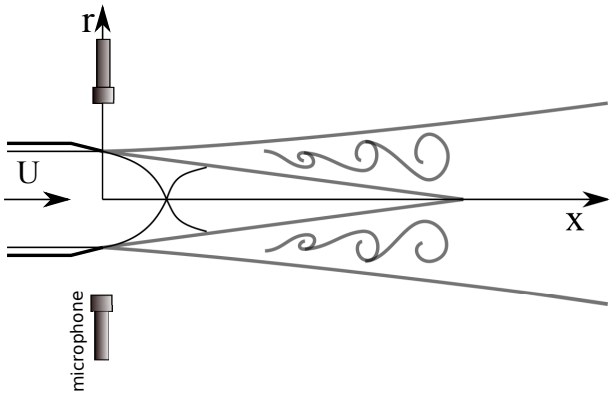

Fig. 3 Schematic representation of the experimental setup and microphone disposition.

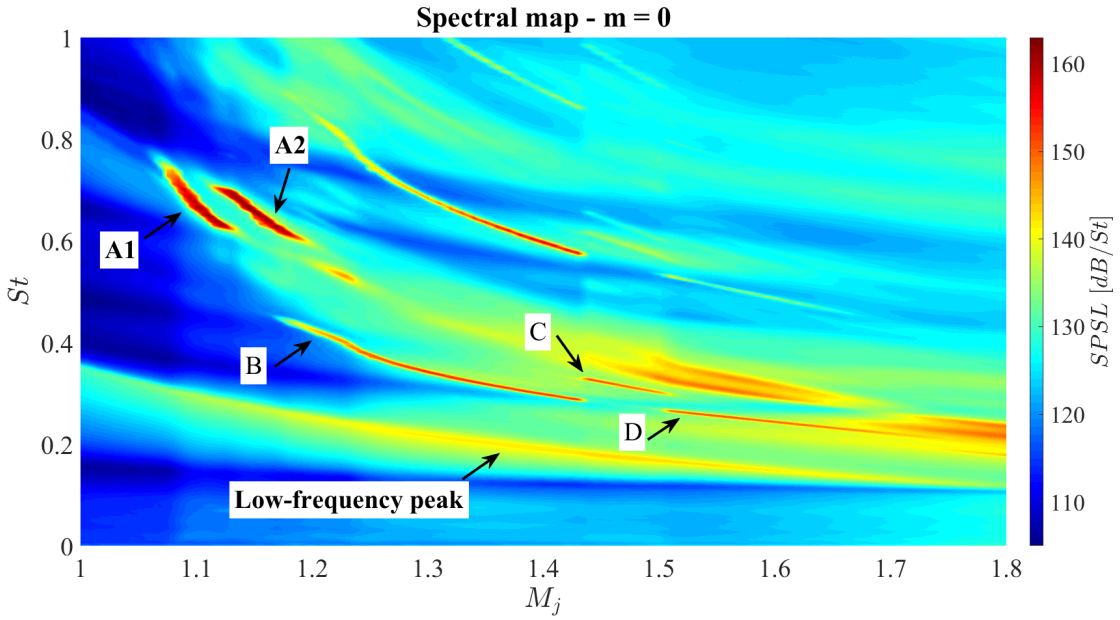

Fig. 4 Spectral map of mode $m = 0$ and detection of screech modes of interest.

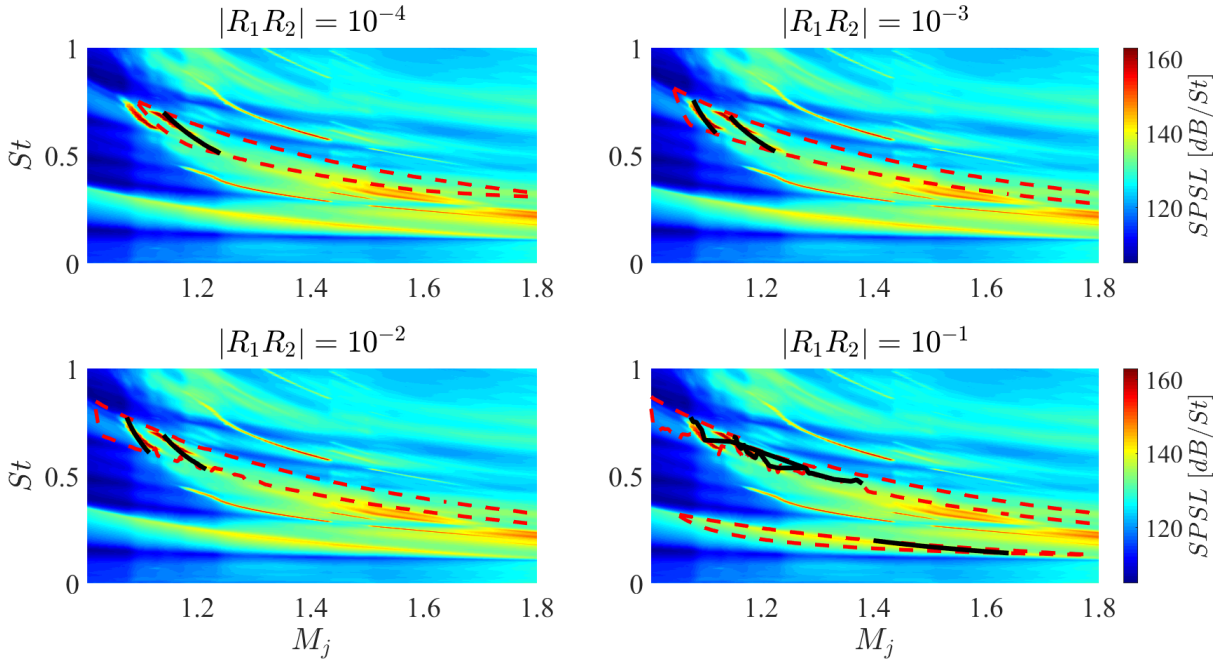

Fig. 5 Spectral maps of mode $m = 0$ and screech-frequency predictions for different values of the amplitude of the reflection coefficient product. Predictions are represented with solid black lines. The region of allowable resonances for which $\omega_i \geq 0$ is marked by dashed red lines.

out-of-phase reflection conditions in eq. (7) and upstream-travelling modes of radial order $n_r = 1$ and 2 for low-frequency and A1-A2 tones, respectively. The threshold frequencies $\omega_r|_{\omega_i=0}$ for all M_j are superimposed on the plot as well. These cut-off/cut-on frequencies define St-M_j region for which $\omega_i \geq 0$ and resonance is not damped. Predictions can be obtained only within this region, whose extension in the St-M_j plane is a function of the amplitude of the reflection coefficient product. We explore four constant values of the reflection coefficient product amplitude, i.e. $|R_1R_2| = 10^{-4}$, 10^{-3}, 10^{-2} and 10^{-1}. We observe that for $|R_1R_2| = 10^{-4}$ the lines individuating $\omega_r|_{\omega_i=0}$ do not include the signature of the A1 screech mode thus preventing the model to predict its resonance frequency. As the amplitude of the reflection coefficient product increases, the region of positive imaginary frequencies becomes wider incorporating allowable resonance frequencies for lower values of M_j. Specifically, the agreement of the resonance predictions of both A1 and A2 modes with the experimental data appears satisfactory for $|R_1R_2| = 10^{-3}$. For the highest value of the reflection coefficient product, i.e. $|R_1R_2| = 10^{-1}$, we notice that the model provides unreliable predictions for the screech modes A1 and A2 and we observe the appearance of an allowable resonance-frequency region delimiting the low-frequency energy peak. Indeed, this peak is well-predicted in the range $M_j = [1.4, 1.65]$. This result implies that $|R_1R_2| = 10^{-1}$ has become too high to sustain resonances for the frequencies and jet flow conditions typical of A1 and A2 modes but suited for the low-frequency energy peak.

A. Predictions with frequency-dependent reflection coefficient product amplitude

The behaviour observed above suggests that the amplitude of the reflection coefficient product should have an increasing trend with the decreasing frequency. This assertion is in agreement with the behaviour observed in other physical systems, such as reflections in hard-walled cylindrical ducts (see among many Silva *et al.* [24]), properties of sound-absorbing materials etc. Based on these evidences and on the results we found, we propose a function $|R_1R_2| = |R_1R_2(St)|$ having an increasing trend for decreasing frequency that fits the reflection coefficient product values which provided predictions at both high and low frequencies in figure 5. We opt for an exponential fit of the kind:

$$|R_1R_2(St)| = a \exp(-b\,St), \tag{8}$$

where a and b are constants obtained by a least mean square optimization. The amplitude of the reflection coefficient product as a function of the frequency is reported in figure 6.

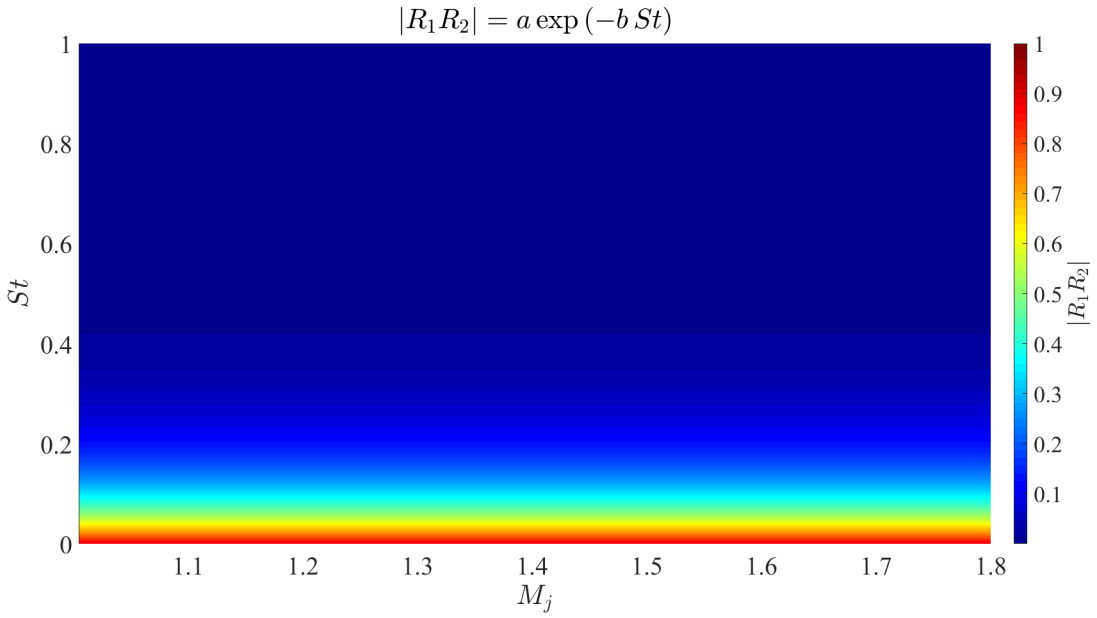

Fig. 6 Representation of the exponential fit based on the experimental results found in figure 5 proposed for the reflection coefficient product along the frequency.

Figure 7 shows the spectral map as a function of St and M_j and the predictions obtained using the exponential shape of the reflection coefficient product along the frequency reported in eq. (8). We observe that the energies of both A1-A2 modes and low-frequency peak are bounded by the $\omega_r|_{\omega_i=0}$ tracks, thus making both the spectral signatures predictable by the resonance model. Specifically, the low-frequency peak is well-predicted for $M_j > 1.4$ and the predictions for A1 and A2 screech modes reproduce well the trend of the experimental data with a lower accuracy in the case of mode A2. This result is ascribed to a not-perfectly suited value of the reflection coefficient product for the frequencies and jet flow conditions typical of mode A2. Indeed, this assertion is also confirmed by the fact that the positive-imaginary-frequency region, and so the region of allowable resonance frequencies, for k_p^- mode of the second radial order extends for St-M_j values where tones are not measured. It is here that the exigence of having a reflection coefficient product function of both St and M_j becomes apparent, as well as the fragility of the complex-frequency analysis due to the treatment of R_1R_2.

Figure 8 shows the contour map of ω_i obtained using the frequency-dependent reflection coefficient product amplitude reported in eq. (8). Screech-frequency and low-frequency peak predictions are superimposed on the plot. We observe that ω_i has a larger value at high frequencies in correspondence of the screech tones than that found at low frequencies. The lower value of ω_i, which corresponds to a lower gain in time in the resonance feedback loop, most likely explains the lower energy amplitude of the low-frequency peak with respect to screech modes A1 and A2.

B. Reflection coefficient product evaluation

In order to try to find a better representation of the reflection coefficient product as a function of both frequency and jet flow conditions, we go back to the real-frequency analysis. We compute the eigenvalues of both the K-H and upstream-travelling modes for $\omega \in \mathcal{R}$ without making the neutral-mode assumption and so considering $k_{KH}^+ \in C$ and $k_p^- \in \mathcal{R}$. We select frequencies for which A1-A2 screech tones and low-frequency peak are measured, we compute the eigenvalues associated with these frequencies and we exploit the resonance condition in eq. (5), i.e. $R_1R_2e^{i\Delta k L_s} = 1$, to calculate $R_1R_2 \in C$. This calculation provides the reflection coefficient product for $\omega_i = 0$, that is without amplification/attenuation in time of the resonance feedback loop, and hence provides the critical or minimum reflection coefficient product to sustain resonance at the St and M_j taken into account.

Figure 9 shows the amplitude of the computed critical reflection coefficient product as a function of St and M_j for the frequencies where tones were measured experimentally. The outcome confirms more or less the order of magnitude of $|R_1R_2|$ that we tested above in the frequency bands of interest. Specifically, we observe that $|R_1R_2|$ increases with decreasing frequency as we assumed in §A and that $|R_1R_2|$ exhibits a decreasing trend with increasing M_j. This result

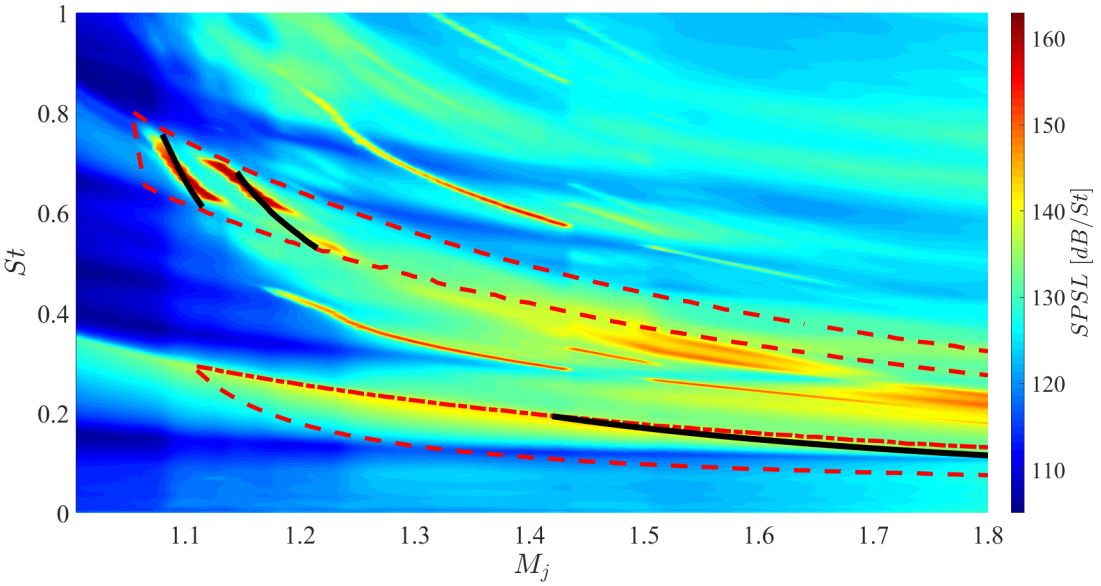

Fig. 7 Spectral map of mode $m = 0$ and predictions obtained considering an exponential trend along the frequency of the amplitude of the reflection coefficient product.

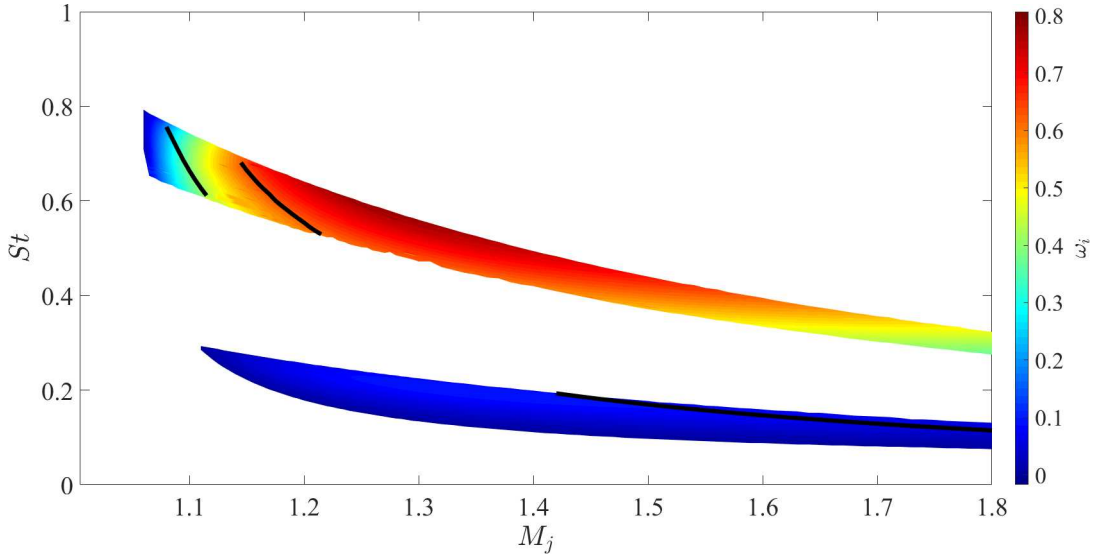

Fig. 8 Contour map of the imaginary frequency for mode $m = 0$ and screech-tone predictions obtained using an exponential fit of the reflection coefficient product amplitude along the frequency.

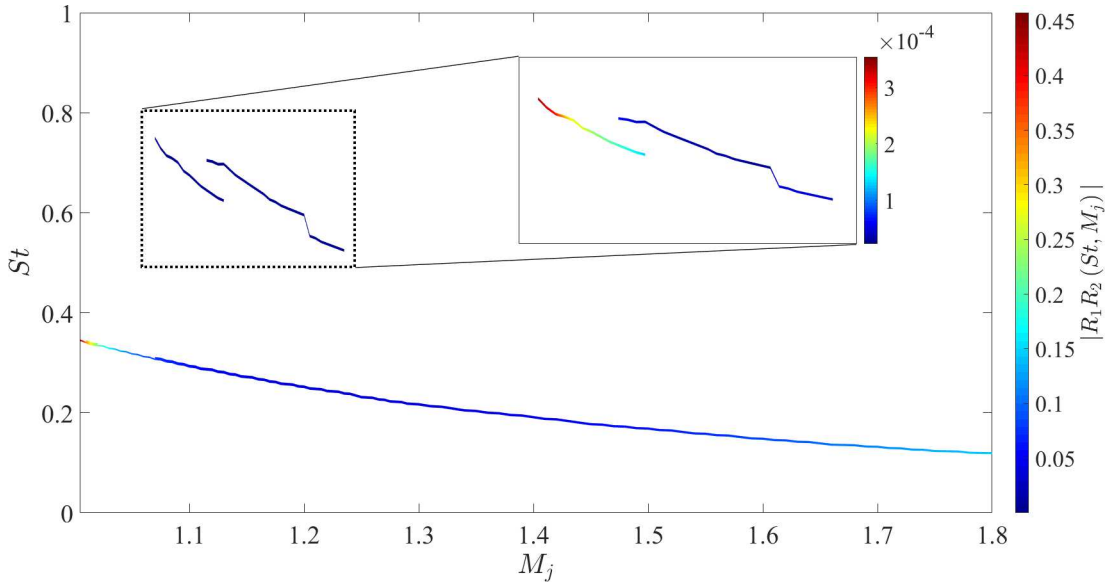

Fig. 9 Representation of the critical or minimum amplitude of the reflection coefficient product computed from eq. (5) **considering** $\omega \in \mathcal{R}$, $k_{KH}^{+} \in C$ **and** $k_p^{-} \in \mathcal{R}$ **for azimuthal mode** $m = 0$**.**

suggests a functional form of $|R_1 R_2\left(M_j\right)|$ to be used in order to define a more accurate reflection coefficient product map as a function of both frequency and flow conditions.

C. Refined screech-frequency predictions

On the basis of the outcome reported in figure 9, we propose here a semi-empirical shape of the amplitude of the reflection coefficient product as a function of both Strouhal and jet Mach numbers. The proposed functional form is:

$$|R_1 R_2\left(St, M_j\right)| = a \exp\left(-b\left(M_j\right) \cdot St^{c\left(M_j\right)}\right) \tag{9}$$

where a, $b\left(M_j\right)$ and $c\left(M_j\right)$ are parameters determined via a least-mean-square-based fit of the critical $|R_1 R_2|$ values in figure 9. We impose a linear trend along the jet Mach number of the coefficients $b\left(M_j\right)$ and $c\left(M_j\right)$. The amplitude of the reflection coefficient product obtained is reported in figure 10. The spectral map and the predictions obtained using $|R_1 R_2| = |R_1 R_2\left(St, M_j\right)|$ are reported in figure 11. Lines indicating $\omega_r|_{\omega_i=0}$ are superimposed on the plot as well. We observe that the regions of the allowable resonance frequencies for both $n_r = 1, 2$ are more tightly-fitted to the measured screech and low-frequency peaks, although a region of $\omega_i \geq 0$ still remains for $n_r = 2$ and high M_j where no tones are measured. Furthermore, the accuracy of the resonance-frequency predictions is higher especially for the screech modes A1 and A2. This result underlines the potentialities of the linear model we propose to correctly describe and model the resonance dynamics of the axisymmetric screech modes.

VI. Conclusions

The resonance tones of the axisymmetric azimuthal mode of a supersonic jet have been modelled. Attention was focused on the A1-A2 screech modes and the low-frequency energy peak measured in the near pressure field of an under-expanded single supersonic jet. The work is a continuation of our recent study [1] in which we proposed a novel screech-frequency prediction model in which closure of the screech resonance loop is provided by upstream-travelling guided jet modes. In this paper we propose a more complete model in which both wavenumber and frequency are complex quantities. The model can provide a more complete description of what is observed experimentally, but to do so it requires knowledge of the upstream and downstream reflection coefficients, which appear in the model as the product $R_1 R_2$. We treat this as a parameter. Results suggest the frequency and Mach number dependence of the reflection-coefficient product and a functional form is proposed that provides good agreement with measurements.

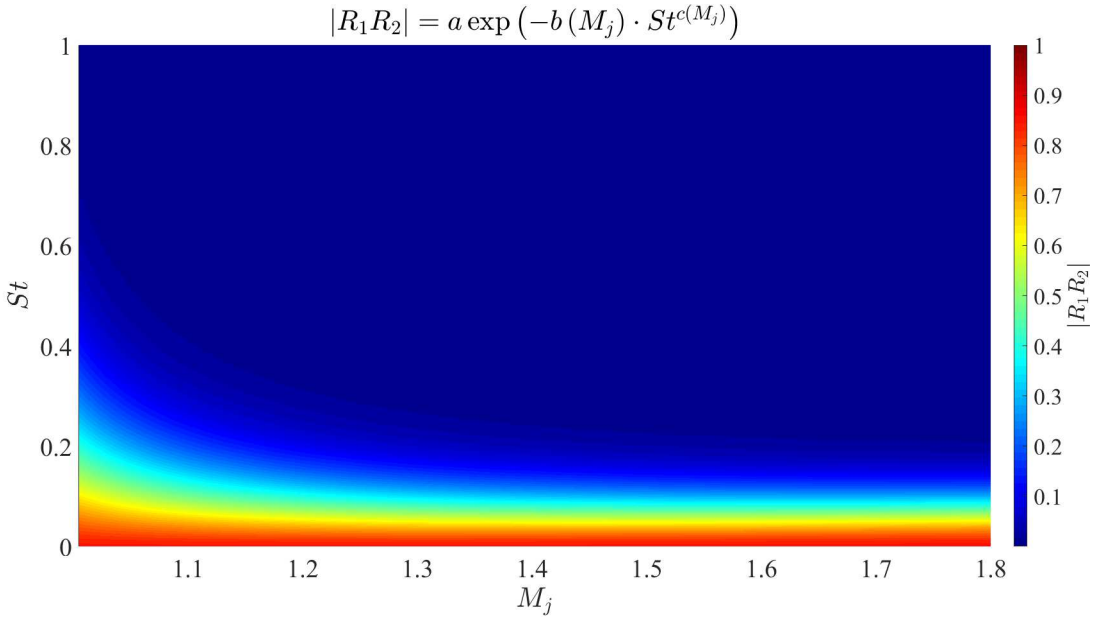

Fig. 10 Representation of the semi-empirical shape of the reflection coefficient product amplitude as a function of both St and M_j based on the trend of the critical $|R_1R_2|$ reported in figure 9.

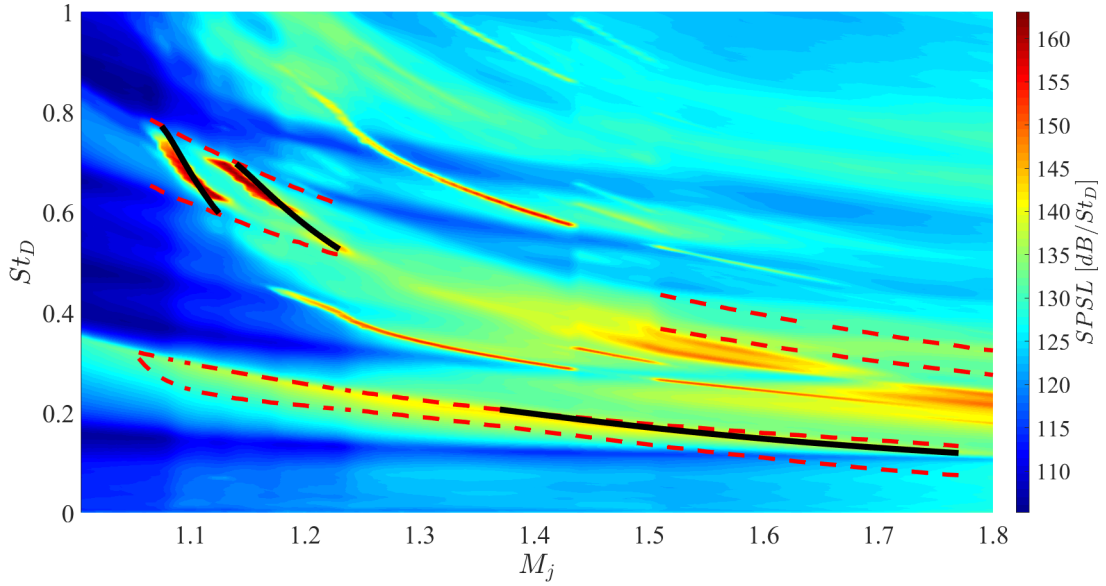

Fig. 11 Spectral map of azimuthal mode $m = 0$ and screech-tone predictions obtained using a reflection coefficient product amplitude function of both Strouhal and jet Mach numbers. Solid black lines represent screech-frequency and low-frequency peak predictions, dashed red lines delimit the St-M_j region where $\omega_i \geq 0$.

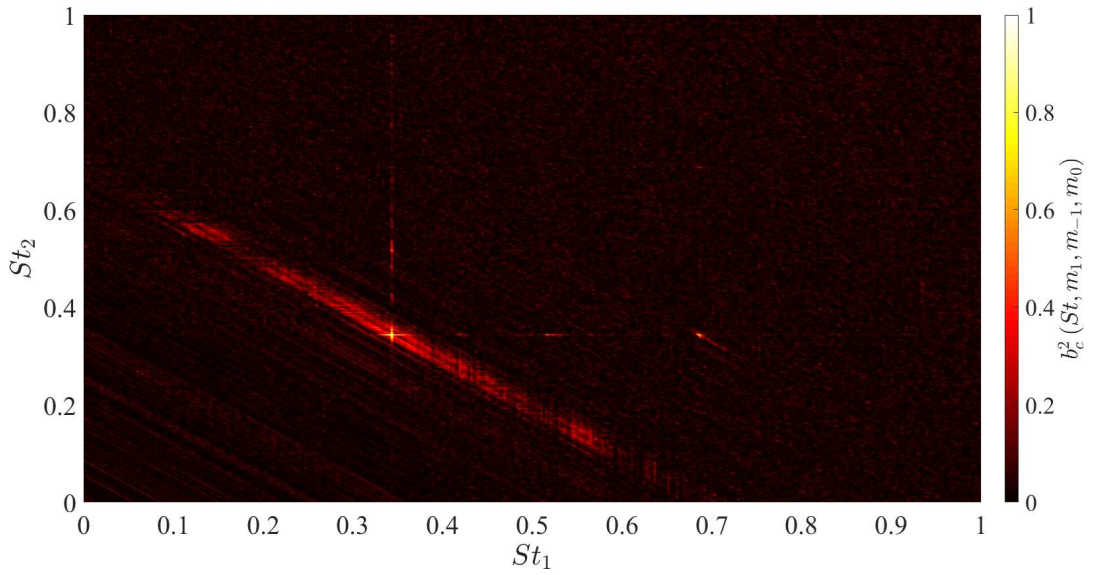

Fig. 12 Cross-bicoherence between azimuthal modes $m = 1$, $m = -1$ and $m = 0$ for jet Mach number $M_j = 1.3$.

Appendix

The rising up of the footprint of the asymmetric B, C and D modes in the spectral content of mode $m = 0$ due to non-linear interaction between modes $m = 1$ and $m = -1$ was proved computing the cross-bicoherence between these azimuthal modes. Non-linear quadratic interaction between azimuthal modes occurs when $m_1 + m_{-1} - m_0 = 0$. Accordingly, the cross-bispectrum is computed as follows [25],

$$B_c\left(f, m_1, m_{-1}, m_0\right) = \langle \hat{p}_1\left(f\right) \hat{p}_{-1}\left(f\right) \hat{p}_0^*\left(f\right) \rangle \tag{10}$$

where $\hat{p}_m\left(f\right)$ is the Fourier transform of the m^{th} azimuthal mode and the superscript $*$ indicates complex conjugate. The cross-bicoherence is obtained normalising the cross-bispectrum as follows,

$$b_c^2\left(f, m_1, m_{-1}, m_0\right) = \frac{\left|B_c\left(f, m_1, m_{-1}, m_0\right)\right|^2}{\langle \left|\hat{p}_0\left(f\right)\right|^2 \rangle \langle \left|\hat{p}_1\left(f\right) \hat{p}_{-1}\left(f\right)\right|^2 \rangle} \tag{11}$$

Figure 12 shows the cross-bicoherence as a function of Strouhal number between azimuthal modes $m = 1$, $m = -1$ and $m = 0$ for $M_j = 1.3$. For this jet Mach number only screech mode B is active and its signature should be found in $m = 1$ and $m = -1$ modes. We observe that a unitary bicoherence level is found for $St_1 = St_2 \approx 0.34$. This implies that a strong non-linear interaction occurs between modes $m = 1$ and $m = -1$ at the frequency component $St \approx 0.34$ leading to the appearance of an energy signature in mode $m = 0$ for such frequency content, as confirmed by figure 4. We also observe a lower bicoherence level for frequency components $St_1 \approx 0.68$ and $St_2 \approx 0.34$ related to the interaction of the B screech mode with its first harmonic. The signature of this interaction is detected in the spectral map in figure 4 by the appearance of the first harmonic of B screech mode in the energy content of azimuthal mode $m = 0$.

Acknowledgments

M.M. acknowledges the support of Centre National d'Études Spatiales (CNES) under a post-doctoral grant.

References

[1] Mancinelli, M., Jaunet, V., Jordan, P., and Towne, A., "Screech-tone prediction using upstream-travelling jet modes," *Exp. Fluids*, Vol. 60, No. 1, 2019, p. 22.

[2] Powell, A., Umeda, Y., and Ishii, R., "Observations of the oscillation modes of choked circular jets," *J. Acoust. Soc. Am.*, Vol. 92, No. 5, 1992, pp. 2823–2836.

[3] Powell, A., "On the mechanism of choked jet noise," *Proc. Phys. Soc. London, Sec. B*, Vol. 66, IOP Publishing, 1953, p. 1039.

[4] Tam, C. K. W., Seiner, J. M., and Yu, J. C., "Proposed relationship between broadband shock associated noise and screech tones," *J. Sound Vib.*, Vol. 110, No. 2, 1986, pp. 309–321.

[5] Panda, J., "An experimental investigation of screech noise generation," *J. Fluid Mech.*, Vol. 378, 1999, pp. 71–96.

[6] Gao, J., and Li, X., "A multi-mode screech frequency prediction formula for circular supersonic jets," *J. Acoust. Soc. Am.*, Vol. 127, No. 3, 2010, pp. 1251–1257.

[7] Shen, H., and Tam, C. K. W., "Three-dimensional numerical simulation of the jet screech phenomenon," *AIAA J.*, Vol. 40, No. 1, 2002, pp. 33–41.

[8] Tam, C. K. W., and Hu, F. Q., "On the three families of instability waves of high-speed jets," *J. Fluid Mech.*, Vol. 201, 1989, pp. 447–483.

[9] Tam, C. K. W., and Ahuja, K. K., "Theoretical model of discrete tone generation by impinging jets," *J. Fluid Mech.*, Vol. 214, 1990, pp. 67–87.

[10] Bogey, C., and Gojon, R., "Feedback loop and upwind-propagating waves in ideally expanded supersonic impinging round jets," *J. Fluid Mech.*, Vol. 823, 2017, pp. 562–591.

[11] Towne, A., Cavalieri, A. V. G., Jordan, P., Colonius, T., Schmidt, O., Jaunet, V., and Brès, G. A., "Acoustic resonance in the potential core of subsonic jets," *J. Fluid Mech.*, Vol. 825, 2017, pp. 1113–1152.

[12] Jordan, P., Jaunet, V., Towne, A., Cavalieri, A. V. G., Colonius, T., Schmidt, O., and Agarwal, A., "Jet-flap interaction tones," *J. Fluid Mech.*, Vol. 853, 2018, pp. 333–358.

[13] Edgington-Mitchell, D., Jaunet, V., Jordan, P., Towne, A., Soria, J., and Honnery, D., "Upstream-travelling acoustic jet modes as a closure mechanism for screech," *J. Fluid Mech.*, Vol. 855.

[14] Gojon, R., Bogey, C., and Mihaescu, M., "Oscillation Modes in Screeching Jets," *AIAA J.*, 2018, pp. 1–7.

[15] Lessen, M., Fox, J. A., and Zien, H. M., "On the inviscid stability of the laminar mixing of two parallel streams of a compressible fluid," *J. Fluid Mech.*, Vol. 23, No. 2, 1965, pp. 355–367.

[16] Michalke, A., "A Note on the Spatial Jet-lnstability of the Compressible Cylindrical Vortex Sheet," Tech. rep., DLR, 1970.

[17] Mercier, B., Castelain, T., and Bailly, C., "Experimental characterisation of the screech feedback loop in underexpanded round jets," *J. Fluid Mech.*, Vol. 824, 2017, pp. 202–229.

[18] Pack, D. C., "A note on Prandtl's formula for the wave-length of a supersonic gas jet," *Q. J. Mech. Appl. Math.*, Vol. 3, No. 2, 1950, pp. 173–181.

[19] Harper-Bourne, M., "The noise from shock waves in supersonic jets-Noise mechanism," *Agard Cp-131*, Vol. 11, 1974, pp. 1–13.

[20] Landau, L. D., and Lifshitz, E. M., *Course of theoretical physics*, Elsevier, 2013.

[21] Mancinelli, M., Pagliaroli, T., Camussi, R., and Castelain, T., "On the hydrodynamic and acoustic nature of pressure proper orthogonal decomposition modes in the near field of a compressible jet," *J. Fluid Mech.*, Vol. 836, 2018, pp. 998–1008.

[22] Pierce, A. D., and Beyer, R. T., *Acoustics: An Introduction to Its Physical Principles and Applications*, 1989$^{\text{th}}$ ed., Acoustical Society of America, 1990.

[23] Pagliaroli, T., Mancinelli, M., Troiani, G., Iemma, U., and Camussi, R., "Fourier and wavelet analyses of intermittent and resonant pressure components in a slot burner," *J. Sound Vib.*, Vol. 413, 2018, pp. 205–224.

[24] Silva, F., Guillemain, P., Kergomard, J., Mallaroni, B., and Norris, A. N., "Approximation formulae for the acoustic radiation impedance of a cylindrical pipe," *J. Sound Vib.*, Vol. 322, No. 1-2, 2009, pp. 255–263.

[25] Panickar, P., Srinivasan, K., and Raman, G., "Nonlinear interactions as precursors to mode jumps in resonant acoustics," *Physics of Fluids*, Vol. 17, No. 9, 2005, p. 096103.